

Electronic Supporting Information

Sulfur-eugenol allyl ether copolymer: A material synthesized via inverse vulcanization from renewable resources and its application in Li-S batteries

Alexander Hoefling,^{‡,a} Dan Thien Nguyen,^{‡,b} Young Joo Lee,^c Seung-Wan Song,^b Patrick Théato^{*,a}

^a Institute for Technical and Macromolecular Chemistry, University of Hamburg, Bundesstr. 45, 20146 Hamburg, Germany.

^b Department of Chemical Engineering and Applied Chemistry, Chungnam National University Daejeon, 305-764, Republic of Korea.

^c Institute of Inorganic and Applied Chemistry, University of Hamburg, Martin-Luther-King-Platz 6, 20146 Hamburg, Germany.

Number of pages: 12

Number of figures: 13

Number of tables: 1

Table of Contents

1. Experimental part.....	1
1.1. Materials.....	1
1.2. Inverse vulcanization of sulfur and eugenol (denoted as S-Eg).....	1
1.3. Synthesis of eugenol allylether:.....	1
1.4. Synthesis of soluble poly(S-co-EAE).....	2
1.5. Preparation of poly(S-co-EAE) cathodes with PVDF as binder.....	2
2. Methods	2
3. Characterization of S-Eugenol-composites.....	3
3.1. ¹ H-NMR experiments.....	3
3.2. FT-IR spectroscopy.....	4
3.3. Thermogravimetric analysis (TGA)	4
3.4. Differential scanning calorimetry (DSC).....	5
3.5. Size exclusion chromatography (SEC).....	6
3.6. Solubility test.....	6
4. Characterization of poly(S-co-EAE).....	7
4.1. Elemental analysis	7
4.2. Solid-state NMR experiments.....	8
4.3. DSC results.....	8
4.4. ¹ H-NMR of soluble poly(S-co-EAE).....	9
4.5. SEC-measurements of soluble poly(S-co-EAE).....	10
4.6. Microstructure of poly(S-co-EAE)	11
5. Electrochemical characterization of poly(S-co-EAE).....	12
5.1. Cycling performance of poly(S-co-EAE) cathodes with PVDF binder.....	12
5.2. Electrochemical reactions	13

1. Experimental part

1.1. Materials

Sulfur (99.95 %, Carl Roth); eugenol (98 %, Sigma-Aldrich); iso-eugenol (Merck); allylbromide (97 % Sigma-Aldrich); dry acetone (Applichem); 1,3-dioxolane (DOX), 1,2-dimethoxyethan (DME), *N*-methylpyrrolidinone (NMP) (over molecular sieve, Acros); lithium-foil (Alfa Aesar); poly(vinylidene fluoride) ($M_w \sim 530k$, Sigma-Aldrich); sodium carboxymethyl cellulose (CMC, $M_w \sim 250k$, Sigma-Aldrich) and polyacrylic acid (PAA, $M_w \sim 450k$, Sigma-Aldrich) and were used as received. Potassium carbonate (Grüssing) was milled and dried at 40°C in vacuum. Bis(trifluoromethane)sulfonimide (LiTFSI) and lithium nitrate (Alfa Aesar) were dried at 40°C in vacuum for several days before use.

1.2. Inverse vulcanization of sulfur and eugenol (denoted as S-Eg)

Elemental sulfur and eugenol were combined in a 20 mL glass vial equipped with a magnetic stirring bar at a 5 g scale. Under vigorous stirring, the mixture was heated at 170°C for 60 min in an oil bath, while the color changed from yellow to dark red but no gelation occurred. The resulting dark red glassy materials changed into yellow composites within 24 h. Samples with 10, 20, 30, 40 and 50 wt% eugenol were prepared.

1.3. Synthesis of eugenol allylether:

Eugenol allylether (EAE) was prepared in a standard William ether synthesis. Under nitrogen atmosphere, 25.1 g (153 mmol, 1 eq) eugenol, 25.4 g (184 mmol, 1.2 eq) potassium carbonate and 100 mL dry acetone were combined in a 500 mL schlenk flask. While stirring, 20.4 g (168 mmol, 1.1 eq) allyl bromide was added dropwise over a syringe. The mixture was heated under reflux overnight. After cooling down to room temperature, 100 mL of 1M NaOH was added. The resulting solution was extracted with 50 mL diethyl ether three times. The organic fractions were combined and dried over $MgSO_4$. The solvent was removed and the residual yellow oil was purified via column chromatography (silica gel, ethyl acetate : petrol ether 1 : 20, $R_f = 0,5$). 18.2 g (89.2 mmol, 58 %) of a colorless oil was obtained.

1H NMR (400 MHz, $CDCl_3$, $\delta = 6.81$ (d, $J = 8.0$ Hz, 1H, Ar-H), 6.73 – 6.67 (m, 2H, Ar H), 6.14 – 6.02 (m, 1H, CH), 6.02 – 5.90 (m, 1H, CH), 5.39 (d, $J = 17.3$ Hz, 1H, CH_2), 5.27 (d, $J = 10.5$ Hz, 1H, CH_2), 5.08 (d, $J = 12.5$, 1H, CH_2), 5.07 – 5.03 (m, 1H, CH_2), 4.59 (d, $J = 5.4$ Hz, 2H, CH_2), 3.86 (s, 3H, CH_3), 3.33 (d, $J = 6.7$ Hz, 2H, CH_2) ppm.

^{13}C -NMR ($CDCl_3$, 101 MHz): $\delta = 149.48, 146.42, 137.77, 133.67, 133.19, 120.44, 117.96, 115.76,$

113.67, 112.32, 70.14, 55.99, 53.57, 39.95 ppm.

GC-MS (EI, pos.): $m/z = 204.184[M]^+$ (calculated for $[C_{13}H_{16}O_2]^+$ 204.115).

1.4. Synthesis of soluble poly(S-co-EAE)

500 mg EAE (2,45 mmol, 1 eq) and 157 mg (4,9 mmol, 2 eq) elemental sulfur were combined in a 5 mL glass vial equipped with a magnetic stirring bar. Under vigorous stirring, the mixture was heated at 175°C in an oil bath for 30 minutes. The color changed to dark brown, but no gelation was observed. After cooling to room temperature, the product was dissolved in methylene chloride (DCM) and precipitated into hexane.

¹H-NMR (CDCl₃, 400 MHz): $\delta = 6.94 - 6.60$ (m, 3H), 6.06 (s, 0.5H), 5.93 (s, 0.2H), 5.38 (d, $J = 16.4$ Hz, 0.4H), 5.28 – 5.23 (m, 0.4H), 5.11 – 4.98 (m, 0.4H), 4.57 (s, .6H), 4.47 – 2.50 (m, 5H), 3.82 (s, 3H), 3.31 (s, 0.6H), 1.52 – 1.22 (m, 1.5H) ppm.

1.5. Preparation of poly(S-co-EAE) cathodes with PVDF as binder

The poly(S-co-EAE) cathodes were prepared by casting a slurry, composed of poly(S-co-EAE) active material, carbon black (Super-C65, Timcal) and poly(vinylidene fluoride) (PVDF, Aldrich, M_w 534,000 $gmol^{-1}$) in a weight ratio of 7 : 2 : 1, dispersed in 1-methyl-2-pyrrolidone (NMP, Acros), onto aluminum foil (30 μ m, Korff AG). The cathodes with a sulfur loading of roughly 0.8 mg cm^{-2} were dried at room temperature for 24 h in high vacuum. In an argon-filled glove box (MBraun, O₂ und H₂O > 0.1 ppm) the cathodes were assembled into CR 2032 coin cells against lithium metal, a separator (PP, 25 μ m, Celgard) and a solution of 2 M lithium bis(trifluoromethane)sulfonamide (LiTFSI, Sigma-Aldrich) and 0.32 M lithium nitrate (LiNO₃, Sigma-Aldrich) in 1,3-dioxolane (DOL, Sigma-Aldrich) and 1,2-dimethoxy ethane (DME, Sigma-Aldrich) at 1 : 1 volume ratio, as electrolyte. Electrochemical charge-discharge cycling ability of poly(S-co-EAE) cathodes was tested in CR 2032 coin cells at a constant current of 0.1 C (167 mA g^{-1}) in the voltage window of 1.7 - 2.6 V on an Arbin BT2143 battery test system. The specific gravimetric capacities of all the cathodes were calculated based on the weight of sulfur.

2. Methods

Attenuated total reflection Fourier transform infrared (ATR-FTIR) spectra were recorded on a Thermo Fisher Scientific Nicolet iS10. Nuclear magnetic resonance (NMR) spectroscopy of solutions was performed on a Bruker Avance 400 MHz FT-NMR spectrometer in deuterated chloroform (CDCl₃) using tetramethylsilane (TMS, $\delta = 0.00$ ppm) as internal standard. Magic angle spinning (MAS) NMR experiments were performed on a Bruker Avance II 400 spectrometer, equipped with a 4mm double

resonance probe. Size exclusion chromatography (SEC) calibrated against polystyrene standards with tetrahydrofuran (THF) as eluent and toluene as internal standard was employed for determination of molecular weights and molecular weight distributions. Elemental Analysis (EA) was carried out on a EuroVector/Hekatech EuroEA Elemental Analyzer. Thermogravimetric analysis (TGA) was performed on a Mettler Toledo "TGA 1" with an Air flow of 20 mL/min and differential scanning calorimetry (DSC) on a "DSC 1" from the same manufacturer, both at a scan rate of 10 K/min.

3. Characterization of S-Eugenol-composites

3.1. $^1\text{H-NMR}$ experiments

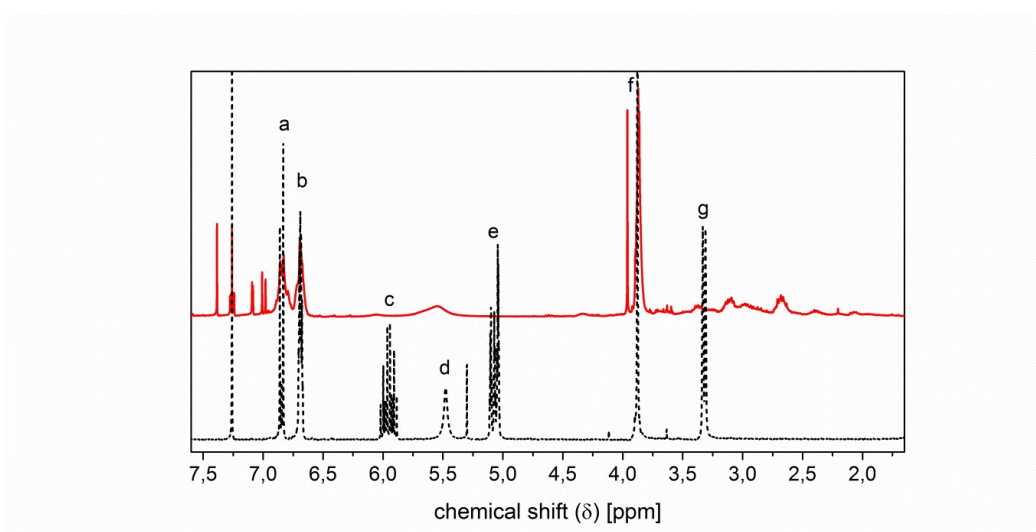


Figure S 1: $^1\text{H-NMR}$ spectra of eugenol (black, dashed line) and S-Eugenol composite with 50 wt% Eugenol content (red, solid line).

The $^1\text{H-NMR}$ spectra clearly indicated the complete conversion through disappearance of the signals corresponding to vinylic proton signals at 5.9 ppm (c) and allylic protons at 5.1 ppm (e). New signals appeared in the range between 4.4 and 2.0 ppm and were attributed to protons of methine and methylene units bearing a (poly-)sulfide unit. Obviously, the hydroxy protons (d) remained after the inverse vulcanization step, showing the tolerance towards this functional group. Further appearance of signals in the aromatic region result from thermally induced rearrangements.

3.2. FT-IR spectroscopy

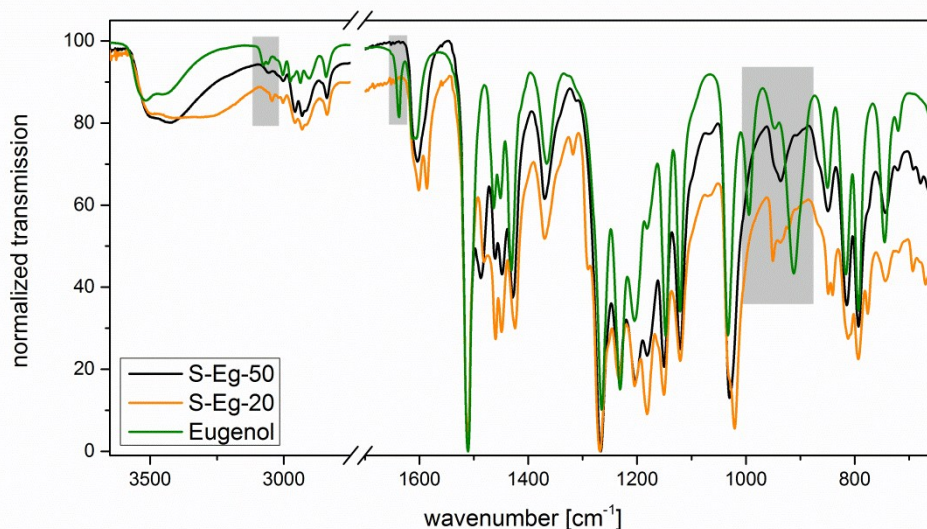


Figure S 2: FT-IR spectra of eugenol and S-eugenol composites (S-Eg-X, with X = eugenol feed ratio).

FT-IR spectra show that the double bonds were fully converted in the resulting composites of the inverse vulcanization of eugenol and elemental sulfur. Signals at 3077 cm^{-1} and 1638 cm^{-1} , representing the stretching vibrations of vinylic C-H bonds and C=C double bonds, respectively, were not observed in the product spectra.

3.3. Thermogravimetric analysis (TGA)

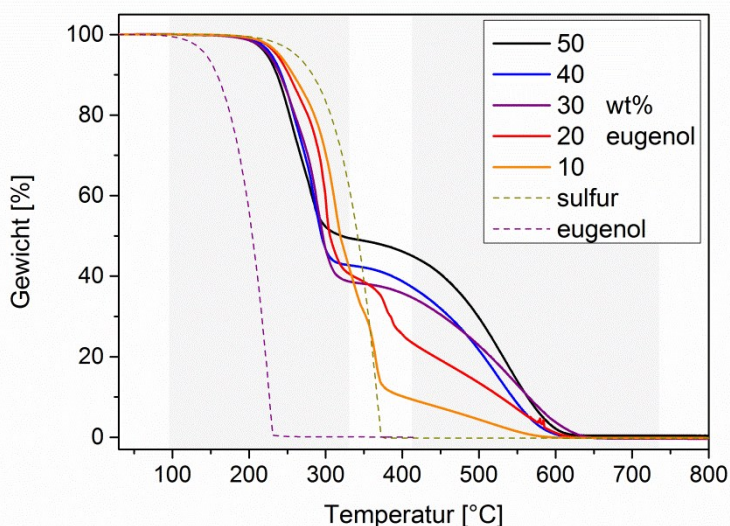


Figure S 3: Thermogravimetric analysis of S-eugenol composites as well as the starting materials sulfur and eugenol.

The S-eugenol composites show an onset temperature for the first degradation step at $\sim 230\text{ °C}$ which is lower than that of elemental sulfur (260 °C) and higher than that of eugenol (140 °C), indicating

successful conversion of both starting materials. The first degradation step can be attributed to the volatilization of sulfur and the second step at higher temperature is correlated with the weight loss of eugenol. A clear dependence of the second step on the eugenol content shows that the feed ratio of eugenol was fully conserved in the composite materials.

3.4. Differential scanning calorimetry (DSC)

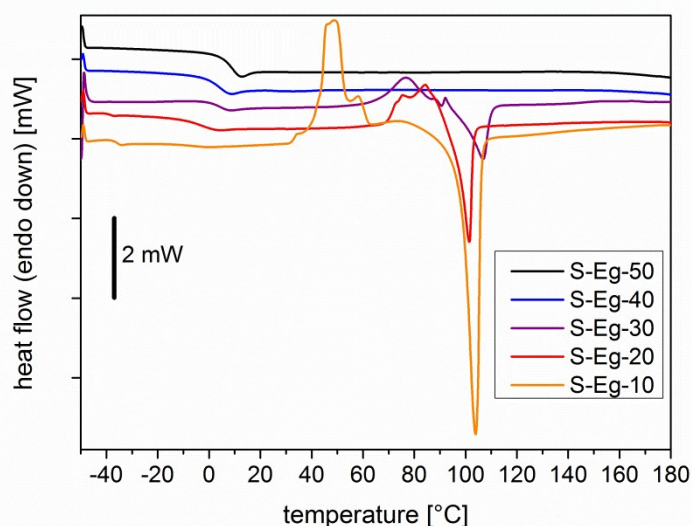


Figure S 4: DSC thermograms of S-eugenol composites (S-Eg-X, with X = eugenol feed ratio).

Crystallization and melting transitions could be observed for S-eugenol composites with less than 40 wt% eugenol content, indicating presence of unconsumed elemental sulfur. In contrast, in the samples S-Eg-40 and S-Eg-50 all the sulfur was consumed. The rise of glass transitions with increasing eugenol feed ratio confirms the conversion and formation of an amorphous phase.

3.5. Size exclusion chromatography (SEC)

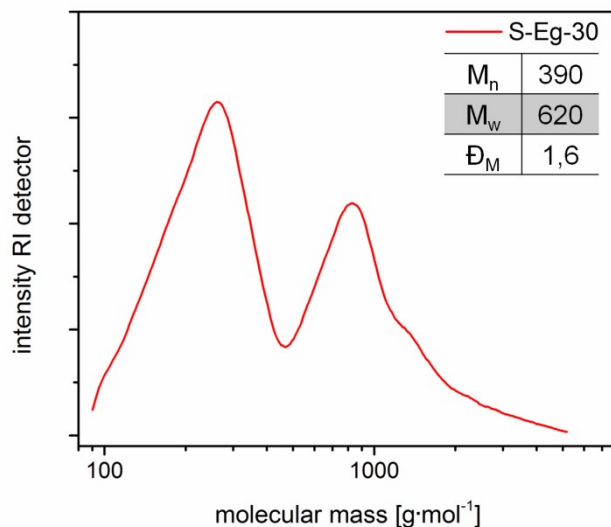


Figure S 5: SEC traces of S-eugenol composite with 30 wt% eugenol.

A bimodal molecular mass distribution is observed, suggesting the formation of simple eugenol-sulfur adducts and oligomers of eugenol and sulfur in the obtained composite materials.

3.6. Solubility test

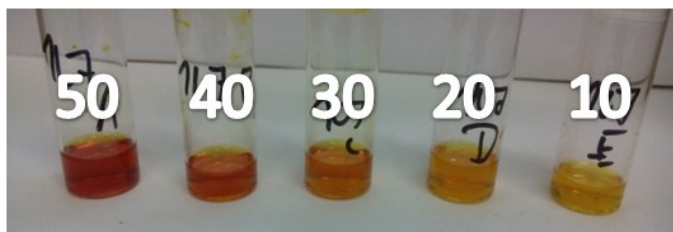


Figure S 6: Solubility test of S-eugenol composites in THF, wt% eugenol stated above.

In accordance to the DSC measurements, it was found that S-eugenol composites with 10 and 20 wt% eugenol were only partially soluble in THF. The samples with eugenol higher than 30 wt% were completely soluble in THF. The sample with 30% eugenol (S-Eg-30) appeared to be soluble judged by the eye, but this might also originate from the low, yet existing, solubility of elemental sulfur in THF.

4. Characterization of poly(S-co-EAE)

4.1. Elemental analysis

Table S 1: Elemental analysis results of Poly(S-co-EAE)

Probe	Element	Calculated from the feed ratio of the synthesis [%]	Observed from Elemental Analysis [%]
S-EAE-10	C	7.64	5.25
	H	0.79	0.67
	S	90.0	92.9
S-EAE-20	C	15.3	12.8
	H	1.58	1.41
	S	80.0	83.5
S-EAE-30	C	22.9	23.8
	H	2.37	2.46
	S	70.0	68.9
S-EAE-40	C	30.6	30.0
	H	3.16	3.07
	S	60.0	60.6
S-EAE-50	C	38.2	38.6
	H	3.95	3.96
	S	50.0	49.1

4.2. Solid-state NMR experiments

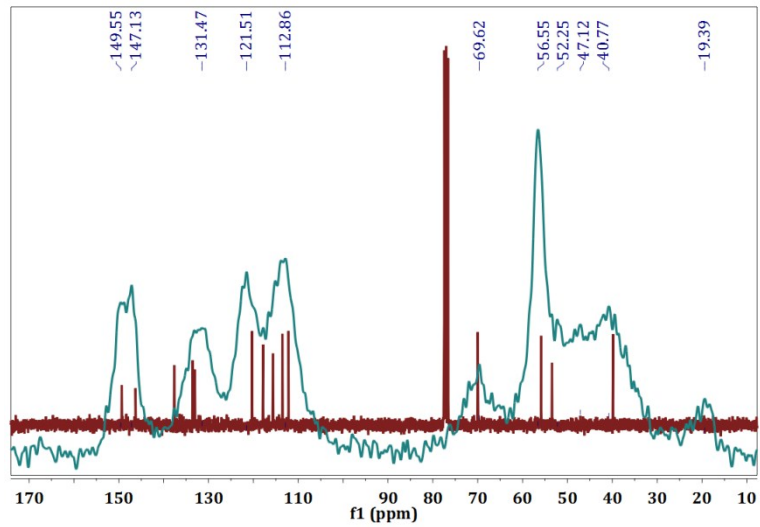


Figure S 7: ^{13}C CP-MAS NMR spectrum of S-EAE-10 (blue line) and ^{13}C -NMR spectrum of EAE (red line).

4.3. DSC results

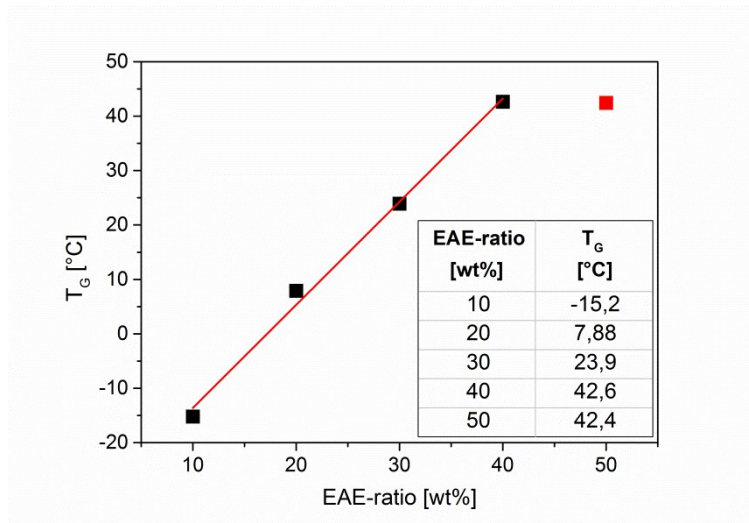


Figure S 8: Linear fit of the glass transition temperatures (T_g) derived from DSC measurements with respect to the EAE-ratio for poly(S-co-EAE) material.

4.4. $^1\text{H-NMR}$ of soluble poly(S-co-EAE)

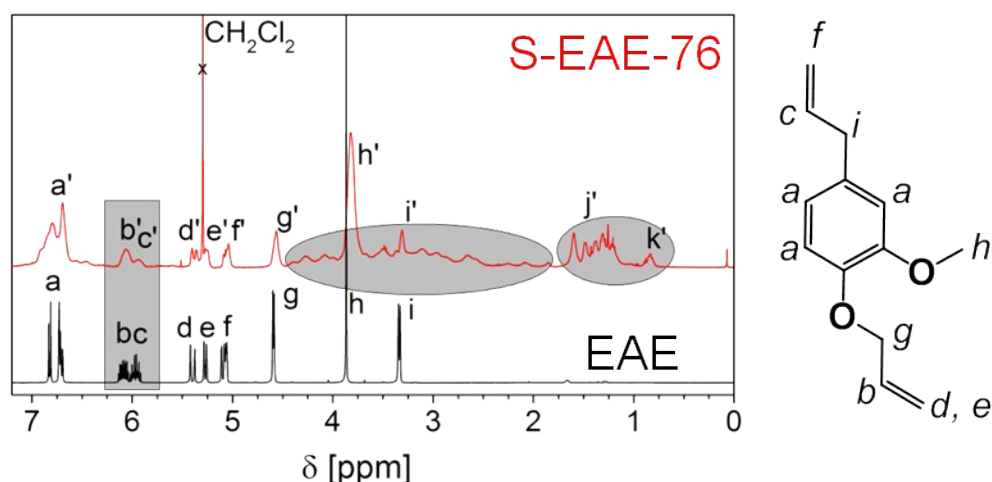


Figure S 9 (a): $^1\text{H-NMR}$ spectra of S-EAE-76 (red line) and EAE (black line).

Similar to the findings for S-eugenol composites, in $^1\text{H NMR}$ spectrum of soluble S-EAE-76, a big variety of ^1H signals appeared in the spectral region between 4.4 and 2.0 ppm (i') that were attributed to protons of methine and methylene units bearing a (poly-)sulfide unit, thereby verifying the formation of a copolymer. However, $^1\text{H NMR}$ signals (b' and c') corresponding to the vinylic protons (b, c) of eugenol allyl ether are still present in the soluble sample, suggesting that some double bonds remain unreacted without formation of C-S linkage. Interestingly, the intensity ratio of these signals has changed to $b' : c' = 2 : 1$, indicating, that the propenyl units are more reactive than the propenoyl groups. Moreover, new signals j' and k' were observed in the product that indicated the formation of methylene and methyl units as side products due to hydrogen abstraction in the free radical reaction mechanism, respectively (Figure S 9b).

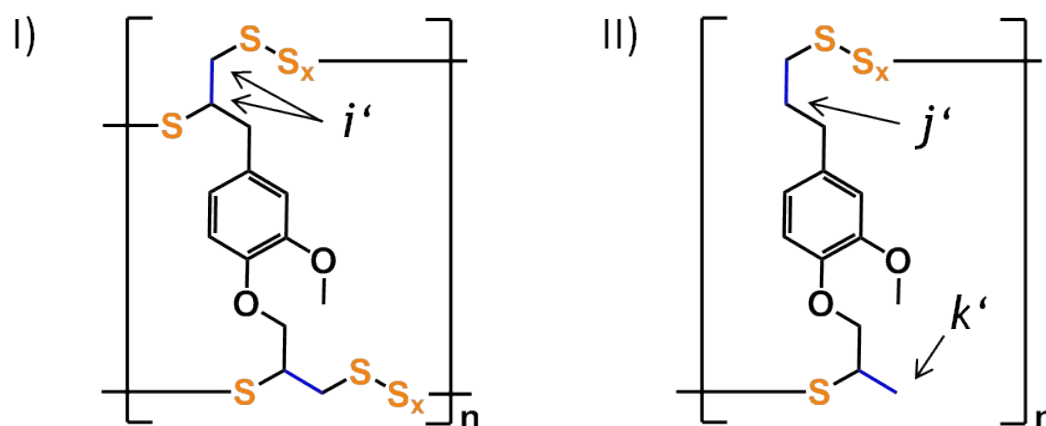


Figure S 9 (b): Proposed substructure units of poly(S-co-EAE) I) without side reaction, II) considering hydrogen abstraction.

4.5. SEC-measurements of soluble poly(S-co-EAE)

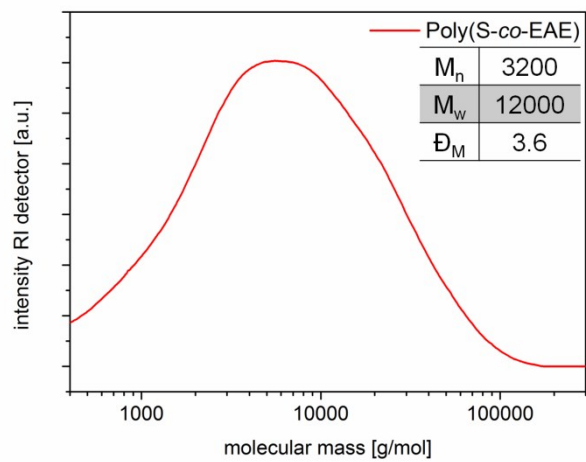


Figure S 10: SEC trace of S-EAE-76, THF as eluent.

4.6. Microstructure of poly(S-co-EAE)

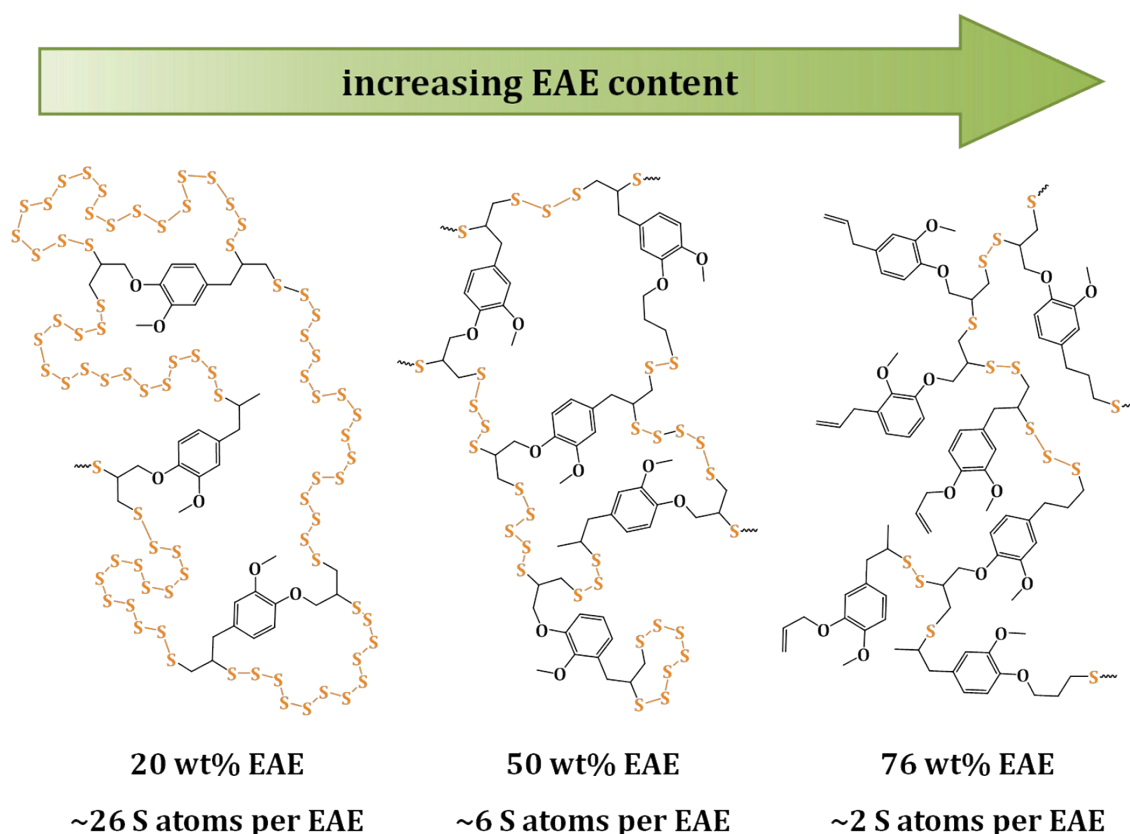


Figure S 11: Schematic representation of the microstructure of poly(S-co-EAE) according to the EAE content.

Based on the presented analysis results we derived an image of the microstructure with respect to the EAE content. Low EAE feed ratios result in rather macrocyclic structures with only few branches containing high-order sulfur chains, in agreement with the low glass transition temperatures (T_g s). An increase of the EAE content represents an increase in the the cross link density in accordance with the linearly ascending T_g s measured. Finally, hyperbranched structures where all the double bonds being consumed and low-order sulfur chains act as the linker between two EAE subunits. Further increase of the EAE content leads to less branched copolymers with alkenyl units as side-chain ends. Earlier discussed rearrangements as well as the observed methyl-group formation were also taken into account.

5. Electrochemical characterization of poly(S-co-EAE)

5.1. Cycling performance of poly(S-co-EAE) cathodes with PVDF binder

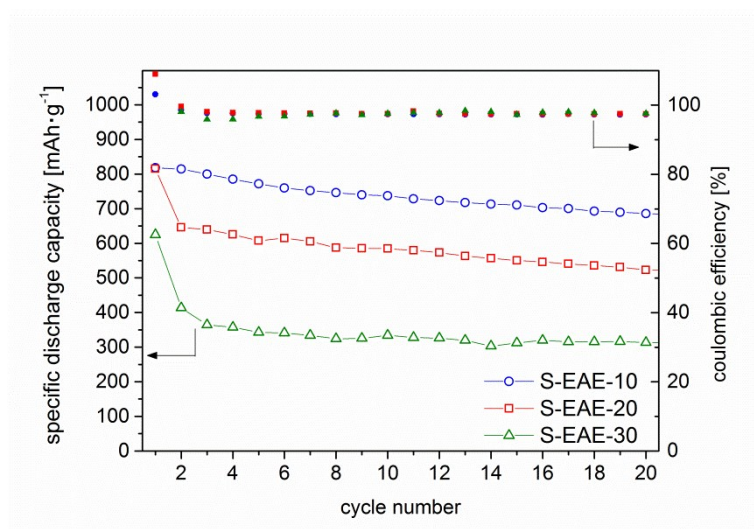


Figure S 12: Cycling performance of poly(S-co-EAE) cathodes with PVDF binder and different EAE content.

The cycling ability of poly(S-co-EAE) cathodes was tested first with cathodes coated with PVdF binder (figure S12). Initial capacities of S-EAE-10, S-EAE-20 and S-EAE-30 were 818 mAhg⁻¹, 815 mAhg⁻¹ and 625 mAhg⁻¹, respectively. However, with increasing EAE content a larger capacity fade after the first cycle was observed, underlining the assumption that the solubility of the reduction products plays a crucial role in terms of capacity retention and is enhanced with increasing EAE content. Coulombic efficiencies were stable at 97 % for all different cathodes. From these preliminary testing, S-EAE-10 performed best, yielding higher capacities and more stable cycling ability than others. To enhance adhesion of the S-EAE-10 cathode active material to the aluminium current collector and between particles of the active material, the aqueous binder with a 1 to 1 mixture of PAA and CMC in water was used, enabling the cathode preparation with water instead of toxic NMP as dispersion medium.

5.2. Electrochemical reactions

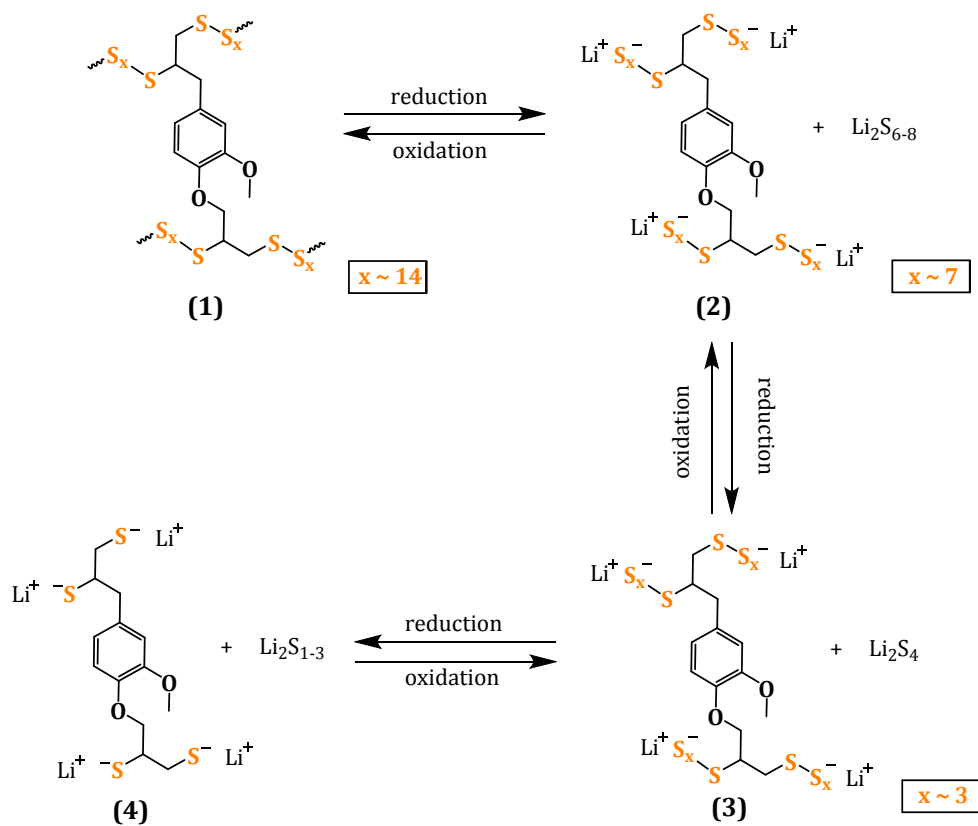


Figure S 13: Schematic overview of the proposed reactions taking place upon reduction (discharge) and oxidation (charge) in poly(S-co-EAE) cathodes.